Protein capped nanosilver free radical oxidation: role of biomolecule capping on nanoparticle colloidal stability and protein oxidation

Manuel Ahumada, Cornelia Bohne, Jessy Oake & Emilio I. Alarcon

April 2018

The final publication is available via Royal Society of Chemistry at:

https://doi.org/10.1039/C7CC08629F

Journal Name

COMMUNICATION

Protein Capped Nanosilver Free Radical Oxidation: Role of the Biomolecule Capping on Nanoparticle Colloidal Stability and Protein Oxidation

Received 00th January 20xx,
Accepted 00th January 20xx

DOI: 10.1039/x0xx00000x

www.rsc.org/

Manuel Ahumada,[a,b*] Cornelia Bohne,[c] Jessy Oake,[c] and Emilio I. Alarcon[a,d,*]

We studied the effect of human serum albumin protein surrounding spherical nanosilver on the nanoparticle stability upon peroxyl radical oxidation. The nanoparticle-proteins composite is less prone to oxidation compared to the individual components. However, higher concentrations of hydrogen peroxide were formed in the nanoparticle-proteins system.

Novel therapies exploring nanoscale interactions for biomedicine have prompted research in nanomaterials. Silver nanoparticles (AgNPs), or nanosilver, have been extensively studied as novel antimicrobial, antibiofilm, and anti-inflammatory agents.[1, 2] We, and others, have demonstrated that surface composition dictates both the nanoparticle's fate within living organisms and its biological activity.[3-6] Such surface composition is by nature dynamic, which in biological system is mainly dominated by interactions with biomolecules.[7] With proteins being the most abundant components in biofluids, nanoparticles' surface composition will become primarily dominated by proteins aggregates adsorbed onto the nanoparticle surface, forming what is known as protein corona.[8-15] Adsorption of proteins onto the nanoparticle surface occurs in steps following a behavior similar to the 'Vroman effect';[16, 17] where the most abundant proteins are the first to adsorb, but equilibrium is ultimately achieved at longer times for biomacromolecules with higher affinities independently of their relative concentration in the biofluid. Added to this already complex multi-step dynamic equilibrium; it has recently reported that nanoparticle shape and size also plays an important role in the total protein landscape and corona formation onto the nanoparticle surface.[18]

With proteins being the primary target for free radical oxidation in living organisms; a logical question to ask is whether nanoparticles "encapsulated" within a corona-like structure can interfere in the protein oxidation, by either reducing or promoting free radical oxidation. Endogenous free radicals, including reactive oxygen species (ROS), are produced continuously as side products of cell metabolism. While damage to proteins and other biomolecules is kept to a minimum under normal conditions thanks to the orchestrated biochemical cell machinery.[19] However, diseases and, or external agents (e.g., chemotherapy) increase the free radical production overwhelming the biochemical mechanisms for minimizing oxidative damage.[20] To date, however, the effect of nanoparticle-protein capped free radical oxidation, and its impact on protein oxidation have not been systematically studied. In the present work, we have used spherical nanosilver that has a high affinity for proteins[21] such as albumins, as a model for exploring the impact of peroxyl radical oxidation, which is primarily responsible for protein and lipid oxidation in biological systems.[22] Peroxyl radicals were generated at a steady rate from the thermal decomposition of 2,2'-azobis(2-methylpropionamidine) dihydrochloride (AAPH, 14nM/s at 37°C, see Scheme 1).[23]

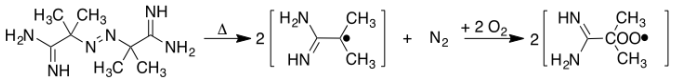

Scheme 1. Chemical reaction of AAPH thermal decomposition and peroxyl radical generation.

Similar to what has been described in the literature for plasmonic absorption of small spherical nanosilver (3-5 nm),[24-27] our citrate capped nanosilver were spherical in shape, see Fig. S1, and showed an intense plasmonic absorption (SPB) at ≈ 395 nm. A nominal 40 nM nanosilver concentration was estimated assuming a monodisperse population centered at 4.0 nm, see SI. Changes in SPB are often used to monitor concentration, size, and polydispersity of metal nanoparticles. In our case, we followed the changes in SPB for citrate capped AgNPs upon addition of 10 mM AAPH, see Fig. 1. The decrease

[a] [a]Division of Cardiac Surgery Research, University of Ottawa Heart Institute, 40 Ruskin Street, Ottawa, Canada. [b]Centro de Nanotecnología Aplicada, Facultad de Ciencias, Universidad Mayor, Camino La Piramide 5750, Huechuraba, Región Metropolitana, 8580745, Chile. [c]Department of Chemistry, University of Victoria, Victoria, BC, Canada. [d]Department of Biochemistry, Microbiology, and Immunology, Faculty of Medicine, University of Ottawa, Ottawa, Canada.
[b] *Corresponding authors e-mail: mahumada@ottawaheart.ca; ealarcon@ottawaheart.ca
[c] Electronic Supplementary Information (ESI) available: Methods and Supplementary Figures. See DOI: 10.1039/x0xx00000x

in the nanoparticle SPB, which ultimately leads to only having the absorption for AAPH at > 60 s (Fig. S2), is accompanied by a broadening of the SPB and an increment in absorption at longer wavelengths >500 nm; an indication of nanoparticle aggregation, Fig. 1 left. To test ionic strength effects, we added 10 mM NaCl leading to only minor variation of the SPB (< 3.0 nm, see Fig. S3).

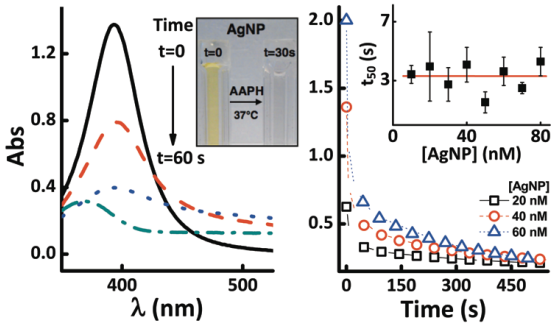

Figure 1. Changes in SPB for citrate-capped silver nanoparticles mediated by peroxyl radicals. **Left**: UV-vis spectral changes over time for 40 nM AgNP@citrate in the presence of 10 mM AAPH at 37°C (spectra recorded at 0, 10, 25 and 60 s); inset shows representative images for the change after 30s incubation of AgNP@citrate with AAPH. **Right**: Kinetics for the decrease of the SPB (λ = 395 nm); inset shows t_{50} values of the oxidation reaction at different AgNP concentrations. Measurements were carried out in triplicate using different nanoparticle batches.

By using the ratio between the average initial rate of SPB decrease for citrate capped AgNP (12 ± 2 nM/s, Fig. 1 right) and the peroxyl radical production rate (14 nM/s at 37°C),[23] one can estimate the ability of AgNPs to act as free radical traps; the calculated free radical efficiency suggests that ≈ 1.0 radical is sufficient to destabilize a multi-atomic nanosilver. In our estimation for the number of free radicals per nanoparticle we have assumed a nanoparticle concentration derived from perfectly monodisperse spherical nanosilver. The fact that t_{50}[§] values remained unchanged for the different AgNPs concentrations tested suggests the involvement of a chain reaction mechanism.

Formation of a supramolecular structure of proteins surrounding nanosilver has been recently reviewed in the literature.[28] Nanosilver protein-like corona structures have been also identified as modulator of sulphidation,[29] nanoparticle toxicity,[30, 31] and availability in biomimetic systems.[32] In our case, the interaction between nanosilver and the protein was estimated by measuring the binding constant (K_a), from monitoring changes in the protein tryptophan (Trp-214) fluorescence (Fig. S4).[24]

Changes in the fluorescence intensities upon addition of AgNPs were analysed using the Stern-Volmer plot (R=0.997; R^2=0.995):

$$F_0/F = 1 + K_{SV}[AgNP] \quad (1)$$

$$K_{SV} = k_q \, x \, \tau_0 \quad (2)$$

A quenching rate constant k_q of 1.4 × 10^{16} M^{-1} s^{-1} was calculated from the Stern-Volmer constant (eq. 2, K_{sv} = (6.5 ± 0.1) × 10^7 M^{-1}), using the reported fluorescence lifetime for HSA (τ_0 ≈ 4.6 ns).[33] This k_q value is several orders of magnitude higher than the diffusion controlled limit in water ≈ 1 x 10^{10} M^{-1} s^{-1},[34] which implies nanoparticle and HSA ground-state complex formation. Ultracentrifugation experiments, which have been described to be a useful tool to estimated binding of proteins to nanostructures,[35] were carried out to determine the amount of bound protein to nanosilver. No nanosilver was detected in the supernatant of the ultracentrifuged samples. Total adsorbed protein concentration, at a fixed nanosilver amount, varied depending on the initial protein concentration. Thus, an 80% of the protein was bound when using 1.0 µM of the macromolecule. Increasing the initial protein concentration by tenfold increases in 5.5 times the absorbed protein concentration to 4.4 µM. Further, when considering that the protein size is larger than the nanoparticle (6.6 ± 0.4 vs. 4.2 ± 0.1 nm, see below). The difference in the fraction of bound HSA cannot be explained regarding surface saturation. Thus, the formation of different supramolecular arrangements of HSA around the nanoparticle surface is the most plausible explanation.

Fig. 2 left shows that protein concentrations as low as 1.0 µM decelerate SPB loss in the presence of AAPH. Interestingly, no significant differences in the t50 values for the screened protein concentrations were observed (p>0.1, one way ANOVA, see SI). Similar to the citrate-protected AgNPs, there was a sub-second component for the SPB decrease that for HSA capped AgNPs was also investigated by stopped-flow (SF, see SI for experimental methods). When AgNPs were mixed with water in a control experiment no changes in absorption were observed (Fig. 2 right). In contrast, when AgNPs were combined with NaCl solutions a fast decrease in the SPB was found in the first 0.5s. This fast decrease suggests that after adding NaCl, there is a rapid supramolecular reorganization of the protein molecules around the nanoparticle,[36, 37] which promotes changes in the electronic density of the metal surface and consequently modifies the SPB.[25] This change in the position of the SPB is responsible for the different initial absorbance values when the AgNPs are diluted with water or with NaCl.[§§] At longer time scales changes in the SPB with the addition of NaCl and AAPH differed and the faster rate in the presence of AAPH corresponds to the radical oxidation process. Thus, we used t_{50} values for times >0.5 s, to avoid including the ionic strength effect in the analysis.

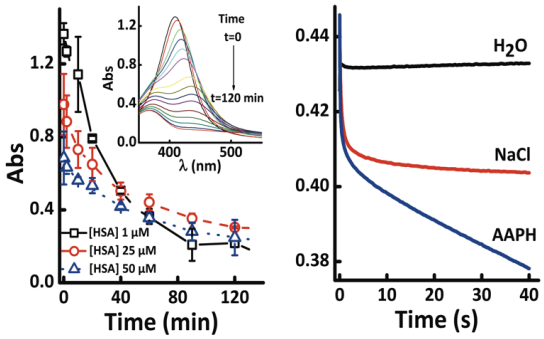

Figure 2. Changes in nanosilver surface plasmon band absorption for HSA capped AgNPs incubated with 10 mM AAPH. **Left:** Changes in SPB for HSA protected AgNP (40 nM) measured up to 120 min after addition of AAPH. The absorption was measured at the maximum SPB for each spectrum (data correspond to the average of 3 independent experiments). Inset: Representative SPB spectra for AgNPs measured in the presence of 10 µM HSA over time (0 to 120 min) after addition of AAPH. **Right:** Representative SPB kinetics for stopped-flow measurements for the AgNP (20 nM) bound to HSA (10 µM) upon addition of water, NaCl or AAPH (kinetic traces correspond to averages of 16 kinetic traces for a single experiment). All measurements were carried out at 37°C. SPB is protein concentration dependent, for λ values see Fig. S4 right.

Adding micromolar concentrations of HSA decelerates the loss in SPB absorption with no differences in slope for all concentrations tested. Thus, if we consider that 100% of the proteins are attached to the AgNPs (≈40 nM, monodisperse spherical), there would be around 25 and 1,250 proteins per nanoparticle at 1 µM and 50 µM of HSA, respectively. While considering geometric restrictions (see SI); only 4 proteins can fit onto the nanoparticle surface. To accommodate 25 protein molecules per nanoparticle the protein-nanoparticle "corona" model can be used. However, having 1,250 proteins associated with the NP is unrealistic. Thus, we further characterized the formation of the nanoparticle-protein supramolecular system under different conditions at 1.0 µM HSA. The measurements of the hydrodynamic size (dynamic light scattering; DLS) and electrokinetic potential (ζ-potential), were used to evaluate aggregation and colloidal stability of nanosilver and has, either separated or combined.

Table 1. Hydrodynamic size (DLS) and ζ -potential of HSA, AgNP and NP-protein composite measured in solution without and with AAPH (10 mM at 37°C pre-incubated for 120 min). Results correspond to the average of 3 independent measurements.

Sample	Size (nm)	ζ -potential (mV)
HSA	6.6 ± 0.4	-8 ± 3
AgNP	4.2 ± 0.1	-28 ± 3
AgNP + AAPH	*a*	*a*
AgNP-HSA*	10 ± 1	-23 ± 4
AgNP-HSA* + AAPH	400 ± 40	-17 ± 1

*1.0 µM HSA was used in all experiments. [a]colloid precipitates out of the solution within seconds.

The protein nanoparticle composite has a hydrodynamic size larger than their individual components by separate (10 nm), but still smaller than the sum of their respective hydrodynamic sizes. Those differences might be attributed to conformational changes that occur during the initial interaction between the protein and nanoparticle, similar to what has been described in the literature for the interaction of albumin proteins and nanosilver.[24, 30] Despite in our work we are using only 1 type of protein, HSA, this increment in hydrodynamic size aligns well with the findings for protein corona formation in other metal nanoparticle systems reported in the literature.[38] Incubation of citrate-protected nanoparticles with AAPH leads to the rapid formation of larger aggregates (≈200X original diameter), which aligns well with the changes at longer wavelengths showed in Fig. 1. However, incubating the AgNPs-protein composites with AAPH results in a ≈ 40X increase in the hydrodynamic size. The nanoparticles remain relatively stable for a more extended period in solution as reflected in the sample's zeta potential; a parameter that accounts for colloidal stability.[21]

Trp fluorescence with and without nanosilver incubated with AAPH (Fig. S5 left) was used to follow in situ the free radical oxidation of the only Trp residue in HSA (Trp-214). For the nanoparticle-protein composite, there was a 25% loss in the emission while 70% of the fluorescence disappeared for the protein sample without AgNPs. This behavior points towards a reduction in the Trp oxidation, once the protein assembles around the nanostructure. Ashraf *et al*. have reported similar findings for AgNPs-HSA incubated with methylglyoxal.[39]

The extent of protein fragmentation/cross-linking for the protein capped nanomaterial incubated with 10 mM AAPH was evaluated by SDS-page electrophoresis. Fig. S6 shows no significant differences after 2h of incubation in the presence of nanosilver. We also measured early and late oxidation markers (peroxides and carbonyls, respectively), and oxygen consumption product of the radical production. [22]

No measurable peroxides were detected in the absence of AAPH (Fig. S5 right). However, the peroxide concentration increased 2.5X for AgNPs-HSA when compared to oxidized HSA. The carbonyl content remained mostly unchanged amongst all samples, suggesting peroxides do not evolve to the formation of carboxyl end products or that such peroxides fraction corresponds to hydrogen peroxide. Oxygen consumption was 25% slower for AgNPs-HSA compared to HSA alone. These results point towards chain oxidation reaction of the protein promoted by the nanoparticle acting as a trap that constrains a high number of proteins in a limited space. Formation of hydrogen peroxide during protein oxidation was assessed by following changes in the oxygen concentration of the systems upon adding catalase (100 U/mL), which decomposes hydrogen peroxide to water and molecular oxygen (see Fig. S7). The oxygen concentration upon adding the enzyme increased only for AgNPs-HSA, which suggests the formation of hydrogen peroxide during the oxidation of the hybrid nanocomposite. This formation of hydrogen peroxide is in agreement with literature reports that have suggested that metal nanosurfaces actively participate in hydrogen peroxide production.[40]

In summary, by using HSA as a protein model for nanosilver capping, we demonstrated that the formation of protein layer onto nanosilver not only improves the nanoparticle colloidal stability but also affects the protein oxidation profile and extent. Thus, upon exposing the system to radicals, tryptophan oxidation was lower for the protein when capping nanosilver. This oxidation was accompanied by a 2.5 times increment in peroxides, most likely hydrogen peroxide. The ability to accumulate peroxides for the protein-nanosilver composite under oxidative stress might also be linked to the antibacterial effects in vivo displayed by nanosilver.[3] Thus, the proteins

surrounding the nanosurface act as shields from exogenous reactive species in a similar fashion as the ancient Roman army formed a "Testudo formation." Despite that additional work for further understanding to link surface reactivity and the nanoparticle biologically activity is required; our work constitutes a building block in the way to better understanding *in vivo* consequences of exposing nanomaterials to free radicals in living organisms.

This work was supported by NSERC Discovery, the Canadian Institutes of Health Research and University of Ottawa Heart Institute to EIA. The work at the University of Victoria was supported by an NSERC Discovery Grant (RGPIN-121389-2012).

Notes and references

§ The parameter t_{50} corresponds to the time required to reach half of the absorbance amplitude where the minimum absorbance corresponds to the final absorbance of AAPH.

§§ The control experiment with NaCl was required because in the addition of AAPH the ionic strength of the solution was increased by 200 times.

1. H. de Alwis Weerasekera, M. Griffith and E. I. Alarcon, in *Silver Nanoparticle Applications: In the Fabrication and Design of Medical and Biosensing Devices*, eds. E. I. Alarcon, M. Griffith and K. I. Udekwu, Springer International Publishing, Cham, 2015, pp. 93-125.
2. L. Rizzello and P. P. Pompa, *Chem. Soc. Rev.*, 2014, **43**, 1501-1518.
3. M. Griffith, K. I. Udekwu, S. Gkotzis, T.-F. Mah and E. I. Alarcon, in *Silver Nanoparticle Applications: In the Fabrication and Design of Medical and Biosensing Devices*, eds. E. I. Alarcon, M. Griffith and K. I. Udekwu, Springer International Publishing, Cham, 2015, pp. 127-146.
4. A. Ravindran, P. Chandran and S. S. Khan, *Coll. Surf. B.*, 2013, **105**, 342-352.
5. Y. H. Lim, K. M. Tiemann, G. S. Heo, P. O. Wagers, Y. H. Rezenom, S. Zhang, F. Zhang, W. J. Youngs, D. A. Hunstad and K. L. Wooley, *ACS Nano*, 2015, **9**, 1995-2008.
6. S. McLaughlin, M. Ahumada, W. Franco, T.-F. Mah, R. Seymour, E. J. Suuronen and E. I. Alarcon, *Nanoscale*, 2016, **8**, 19200-19203.
7. S. Wan, P. M. Kelly, E. Mahon, H. Stockmann, P. M. Rudd, F. Caruso, K. A. Dawson, Y. Yan and M. P. Monopoli, *ACS Nano*, 2015, **9**, 2157-2166.
8. T. Cedervall, I. Lynch, S. Lindman, T. Berggård, E. Thulin, H. Nilsson, K. A. Dawson and S. Linse, *PNAS*, 2007, **104**, 2050-2055.
9. I. Lynch and K. A. Dawson, *Nano Today*, 2008, **3**, 40-47.
10. A. E. Nel, L. Madler, D. Velegol, T. Xia, E. M. V. Hoek, P. Somasundaran, F. Klaessig, V. Castranova and M. Thompson, *Nat. Mater.*, 2009, **8**, 543-557.
11. M. P. Monopoli, D. Walczyk, A. Campbell, G. Elia, I. Lynch, F. B. Bombelli and K. A. Dawson, *J. Am. Chem. Soc.*, 2011, **133**, 2525-2534.
12. M. P. Monopoli, C. Aberg, A. Salvati and K. A. Dawson, *Nature Nanotech.*, 2012, **7**, 779-786.
13. C. Gunawan, M. Lim, C. P. Marquis and R. Amal, *J. Mat. Chem. B.*, 2014, **2**, 2060-2083.
14. P. d. Pino, B. Pelaz, Q. Zhang, P. Maffre, G. U. Nienhaus and W. J. Parak, *Materials Horizons*, 2014, **1**, 301-313.
15. C. Corbo, R. Molinaro, A. Parodi, N. E. T. Furman, F. Salvatore and E. Tasciotti, *Nanomedicine*, 2016, **11**, 81-100.
16. L. Vroman, *Nature*, 1962, **196**, 476-477.
17. L. Vroman and A. L. Adams, *J. Biomed. Mat. Res.*, 1969, **3**, 43-67.
18. R. Garcia-Alvarez, M. Hadjidemetriou, A. Sanchez-Iglesias, L. M. Liz-Marzan and K. Kostarelos, *Nanoscale*, 2018, **10**, 1256-1264.
19. R. L. Auten and J. M. Davis, *Pediatr. Res.*, 2009, **66**, 121-127.
20. K. J. Davies, *Arch. Biochem. Biophys*, 2016, **595**, 28-32.
21. M. Ahumada, E. Lissi, A. M. Montagut, F. Valenzuela-Henriquez, N. L. Pacioni and E. I. Alarcon, *Analyst*, 2017, **142**, 2067-2089.
22. M. J. Davies, *Biochem. J*, 2016, **473**, 805-825.
23. E. Niki, *Methods Enzymol.*, 1990, **186**, 100-108.
24. E. Alarcon, C. Bueno-Alejo, C. Noel, K. Stamplecoskie, N. Pacioni, H. Poblete and J. C. Scaiano, *J. Nanopart. Res.*, 2013, **15**, 1-14.
25. K. Stamplecoskie, in *Silver Nanoparticle Applications: In the Fabrication and Design of Medical and Biosensing Devices*, eds. E. I. Alarcon, M. Griffith and K. I. Udekwu, Springer International Publishing, Cham, 2015, pp. 1-12.
26. H. Poblete, A. Agarwal, S. S. Thomas, C. Bohne, R. Ravichandran, J. Phospase, J. Comer and E. I. Alarcon, *Langmuir,*, 2016, **32**, 265-273.
27. M. Ahumada, E. Jacques, C. Andronic, J. Comer, H. Poblete and E. I. Alarcon, *J. Mat. Chem. B.* , 2017, **5**, 8925-8928.
28. N. Durán, C. P. Silveira, M. Durán and D. S. T. Martinez, *J. Nanobiotechnology*, 2015, **13**, 55.
29. T. Miclăuş, C. Beer, J. Chevallier, C. Scavenius, V. E. Bochenkov, J. J. Enghild and D. S. Sutherland, *Nature Comm.*, 2016, **7**, 11770.
30. D. K. Ban and S. Paul, *Coll. Surf. B.*, 2016, **146**, 577-584.
31. J. Gao, L. Lin, A. Wei and M. S. Sepúlveda, *Environ. Sci. Tech. Lett.*, 2017, **4**, 174-179.
32. J. H. Shannahan, X. Lai, P. C. Ke, R. Podila, J. M. Brown and F. A. Witzmann, *PLOS ONE*, 2013, **8**, e74001.
33. G. D. Fasman, CRC Press, Inc., Boca Raton, FL, 1989, p. 91.
34. M. Ahumada, E. Lissi and C. Calderón, *J. Photochem. Photobiol. A*, 2016, **325**, 9-12.
35. A. Bekdemir and F. Stellacci, *Nature Comm.*, 2016, **7**, 13121.
36. C. Pfeiffer, C. Rehbock, D. Hühn, C. Carrillo-Carrion, D. J. de Aberasturi, V. Merk, S. Barcikowski and W. J. Parak, *J. Royal Soc. Interf.*, 2014, **11**, 20130931.
37. S. Pasche, J. Vörös, H. J. Griesser, N. D. Spencer and M. Textor, *J. Phys. Chem. B*, 2005, **109**, 17545-17552.
38. E. Casals, T. Pfaller, A. Duschl, G. J. Oostingh and V. Puntes, *ACS Nano*, 2010, **4**, 3623-3632.
39. J. M. Ashraf, M. A. Ansari, H. M. Khan, M. A. Alzohairy and I. Choi, *Sci. Rep.*, 2016, **6**, 20414.
40. P. P. Fu, Q. Xia, H.-M. Hwang, P. C. Ray and H. Yu, *J. Food Drug Anal.*, 2014, **22**, 64-75.

